Supramolecular Interactions Playing an Integral Role in the Near-Infrared Raman "Excitonic" Enhancement Observed in β-Hematin (Malaria Pigment) and Other Related Heme Derivatives

ARTICLE *in* THE JOURNAL OF PHYSICAL CHEMISTRY B · SEPTEMBER 2010

Impact Factor: 3.3 · DOI: 10.1021/jp102307s · Source: PubMed

Supramolecular Interactions Playing an Integral Role in the Near-Infrared Raman "Excitonic" Enhancement Observed in β-Hematin (Malaria Pigment) and Other Related Heme Derivatives

Ratchadaporn Puntharod,[†,‡] Grant T. Webster,[‡] Mehdi Asghari-Khiavi,[‡] Keith R. Bambery,[‡] Feryal Safinejad,[‡] Shadi Rivadehi,[‡] Steven J. Langford,[‡] Kenneth J. Haller,*[,†] and Bayden R. Wood*[,‡]

School of Chemistry, Institute of Science, Suranaree University of Technology, Nakhon Ratchasima 30000, Thailand, and Centre for Biospectroscopy and School of Chemistry, Monash University, Victoria 3800, Australia

Received: October 26, 2009; Revised Manuscript Received: August 8, 2010

To gain more understanding into the mechanism that enables the dramatic resonant Raman enhancement of totally symmetric modes observed in hemozoin (malaria pigment) and other related heme supramolecular arrays when applying near-infrared excitation wavelengths, the iron(III) porphyrins Fe(TPP)Cl, $[Fe(TPP)]_2O$, Fe(OEP)Cl, and $[Fe(OEP)]_2O$ along with β-hematin (synthetic hemozoin or malaria pigment) were analyzed in the solid state using resonance Raman spectroscopy. The critical finding was that from the model compounds investigated, all except $[Fe(OEP)]_2O$ exhibited the enhancement of the totally symmetric mode ν_4 when exciting the molecules with 782 and 830 nm laser lines. Through a detailed comparison of X-ray crystallographic structures, it is proposed that intermolecular noncovalent interactions play an integral role in enabling excitonic interactions to occur in these heme supramolecular systems. Comparison of the solid- and solution-phase electronic spectra in the near-IR region indicated more absorbance in the solid state between 800 and 900 nm. The electronic spectrum of $[Fe(OEP)]_2O$ shows minimal absorbance in this region compared to that of the other compounds. All heme derivatives investigated have similar structure with a five-coordinate high-spin iron(III) ion. The crystallographic data indicate no significant differences in porphyrin geometry between TPP and OEP derivatives studied. However, $[Fe(OEP)]_2O$ contains less supramolecular interactions in comparison to the other species. The supramolecular bonding enhances the probability of through-space interactions between the transition dipoles from electronic transitions of extended π systems. Our results indicate that the intensity of ν_4 is in part strongly affected by C−H···X hydrogen bonding interactions when X is an electron-donating entity. Such information may have important implications in the design and monitoring of antimalarial drugs that specifically interfere with hemozoin formation.

Introduction

Hemozoin (malaria pigment) is a virtually insoluble byproduct of the catabolism of hemoglobin by the malaria parasite *Plasmodium falciparum* and other species.[1−3] The compound is spectroscopically identical to β-hematin, which was found to be a heme dimer linked via reciprocal carboxylate groups with the dimers in turn linked together into a supramolecular hydrogen-bonded array.[4] The interest in hemozoin stems from the fact that quinoline-based antimalarial drugs are thought to bind to hemozoin, therefore preventing its formation, or capping crystal growth, which results in the buildup of toxic free heme, which can kill the parasite.[5−8] Consequently, knowledge on the electronic, vibronic, and molecular structure of hemozoin could lead to the development of new antimalarial drugs that target and block hemozoin formation. In pursuit of new approaches to examine hemozoin drug interactions and gain more insight into the structure of this important compound, we have been utilizing near-infrared (IR) resonance Raman (RR) spectroscopy.[5,9−11]

RR spectroscopy has long been used to provide structural information on porphyrin moieties including metalloporphyrins and, in particular, iron porphyrins that serve as prosthetic groups for heme proteins.[12] Isotopic substitution studies and theoretical calculations have led to the assignment of many bands in the RR spectra of metalloporphyrins and, in particular, hemes.[13,14] Early RR studies reported that specific vibrational modes are sensitive to both the oxidation state and coordination number of the central metal ion.[15,16] One band designated ν_4, assigned to the totally symmetric $C_\alpha-N$ pyrrole breathing mode,[13] appeared particularly sensitive to oxidation state, shifting in position from ∼1370−1375 cm^{-1} in ferric hemes to ∼1355 cm^{-1} in ferrous hemes as a result of increased back-donation of electron density from Fe d_π (d_{xz}, d_{yz}) to porphyrin π^* molecular orbitals.[16] This band was found generally enhanced in RR spectra of hemoglobin solutions when using excitation wavelengths in resonance with the Soret band at ∼400 nm and diminished when exciting in the vicinity of the Q(0,0) and Q(0,1) bands at ∼540 and 575 nm, respectively.[17,18] The enhancement can be explained through the classical *A*- and *B*-type scattering mechanisms based on the sum-over-states approach to light dispersion derived by Kramers and Heisenberg[19] and Dirac[20] from second-order time-dependent perturbation theory. Albre-

* To whom correspondence should be addressed. Address: Centre for Biospectroscopy and School of Chemistry, P.O. Box 23, Monash University, Victoria 3800, Australia. Tel.: +61 3 9905 5721. Fax: +61 3 9905 4597. E-mail: bayden.wood@sci.monash.edu.au. (B.R.W.); Address: School of Chemistry, Suranaree University of Technology, Nakhon Ratchasima 30000, Thailand. Tel.: 66 + 81-547-5377. Fax: 66 +44-224-185. E-mail: ken.haller@gmail.com (K.J.H.).

† Suranaree University of Technology.

‡ Monash University.

10.1021/jp102307s
Published on Web 08/30/2010

cht[21] modified the dispersion expression to take into account electronic state near-resonance effects, which led to two expressions termed as type *A* and type *B* scattering.

In type *A* scattering or Franck−Condon scattering, only totally symmetric modes are enhanced because these are ineffective in mixing the electronic states. The intensity of a particular band is dependent mainly on the overlap wavefunction integrals between the initial, intermediate, and final vibrational states summed over all of the intermediate states (eq 1). The enhancement of totally symmetric modes in heme solutions is commonly seen when exciting into the 400−500 nm Soret band region.

The Condon approximation leads to the *A* term

$$A_{v'v''} = \frac{1}{\hbar} \sum_{v} (\mu^0_{ge})_\rho (\mu^0_{ge})_\sigma \frac{\langle v'|v\rangle\langle v|v''\rangle}{\upsilon_{ev,gv'} - \upsilon_0 - i\Gamma_e} \qquad (1)$$

where v, v′, and v″ are the initial, intermediate, and final vibrational ground states, μ^0_{ge} is the transition moment at equilibrium geometry, $\upsilon_{ev,gv'}$ is the frequency of the transition between the intermediate $|ev\rangle$ and the initial $|gv'\rangle$ vibronic states, ρ and σ are Cartesian coordinates, υ_0 is the frequency of the laser, and $\langle v|v''\rangle$ represents the overlap of the vibrational state v within the excited electronic state manifold and the vibrational state v″, which is the final state and belongs to the ground electronic state.[22] The squares of these vibrational overlaps are known as Franck−Condon factors and determine the intensities of the vibrational sub-bands contributing to the vibrational progressions in the electronic absorption spectrum. Γ_e is the half-width of the vibrational wavefunction for the excited state and represents the lifetime of the excited state, and $\hbar$ is Plank's constant. Resonance occurs when the incident frequency of the laser approaches the frequency of any vibrational transition within the electronic absorption spectrum. The *A* term enhancement mechanism permits only totally symmetric modes to become enhanced because the *A* term part of the Raman intensity is nonzero only for modes that are displaced in the excited state. Nontotally symmetric modes cannot be enhanced in the excited electronic state because these modes are not displaced in the excited state.[22]

Type *B* scattering involves a vibronic coupling between two allowed excited electronic transitions *e* and *r*. The Albrecht *B* term is then

$$B_{v'v''} = \frac{1}{\hbar} \sum_{v} \frac{H^i_{er}}{E_r - E_e} \frac{(\mu^0_{ge})_\rho (\mu^0_{gr})_\sigma \langle v'|v\rangle\langle v|Q_i|v''\rangle + (\mu^0_{ge})_\sigma (\mu^0_{gr})_\rho \langle v'|Q_i|v\rangle\langle v|v''\rangle}{\omega_{ev,gv'} - \omega_0 - i\Gamma_e} \qquad (2)$$

In this expression, *Q* represents the normal coordinate operator, while the other terms are analogous to those detailed in the *A* term. The coupling is a consequence of a breakdown in the Born−Oppenheimer approximation, which occurs when the matrix element H^i_{er} is nonzero

$$H^i_{er} \equiv \langle \Psi_e | \left(\frac{\partial \hat{H}}{\partial Q_i} \right) | \Psi_r \rangle$$

This matrix element is also responsible for intensity borrowing in the electronic spectra via vibronic coupling of excited electronic states.[22] This energy borrowing along with the *B* term increases in magnitude when the coupled states are close in energy. Type *B* scattering explains the enhancement of nontotally symmetric modes observed when exciting hemes with excitation wavelengths between 500 and 600 nm.

The Raman scattering mechanisms described above are based on segregated monomers. However, it has been proposed that aggregated molecules will have a similar form, assuming that the exciton−vibration interactions and vibrational coupling between the molecules are weak in the aggregate.[23] The exciton model is based on the quantum mechanical premise that electronic energy is distributed throughout the aggregate.[23−27] Aggregated enhanced Raman scattering (AERS) has been proposed to explain the anomalous enhancement observed in cyanine dyes absorbed onto surfaces[23,24,26,28−31] and N-protonated porphyrins[25,27,32] The enhancement of vibrational modes in these cases can be explained in terms of an increase size effect and near-resonance terms in the polarizability.[23] Excitonic coupling will split the electronic states into a broad band of states with different geometries, energies, and oscillator strengths. The Raman intensities for a particular wavelength will then reflect the extent of the excitonic coupling. Exciton-coupling-induced changes on electronic energy levels and spectral line widths need to be considered for molecular aggregates with strong excited-state interactions.[23] Raman scattering from aggregated molecules can be enhanced by the Franck−Condon mechanism when the excitation is in resonance with the molecular exciton absorption band of the aggregates.[23] In addition to the additivity and frequency resonance effects, the *A* term bands owe their existence to nonvanishing overlap integral products involving intramolecular and intermolecular wave functions.[29] The net enhancement of Raman vibrational modes could be attributed to an attenuation of fluorescence upon aggregate formation.[23] The Raman cross section of a molecule in an aggregate can still be described by eq 1, but $\upsilon_{ev,gv'}$ and Γ_e are respectively the 0−0 transition energy and the line width factor corresponding to the excitation from the ground state to a specific exciton state. A recent RR study of hemozoin and β-hematin demonstrated that these compounds produce dramatic enhancement of the totally symmetric mode (ν_4) when irradiated with near-IR excitation wavelengths (782 and 830 nm) well away from the Soret and Q bands. It was postulated that the enhancement was attributable to excitonic interactions occurring throughout the supramolecular array.[10] A small broad band centered at 867 nm was observed to shift upon formation of β-hematin from hemin. This was tentatively assigned to a *z*-polarized charge-transfer transition $d_{xy} \rightarrow e_g(\pi^*)$ and implicated as a potential molecular exciton absorption band for AERS. To further investigate the enhancement of ν_4, we have analyzed a number of structurally related high-spin ferric hemes with RR spectroscopy and correlated these results with X-ray crystallographic structural results.

RR spectra of model heme complexes including iron tetraphenylporphyrin Fe(TPP) and iron octaethylporphyrin Fe(OEP) derivatives in both monomeric and dimeric forms have been extensively studied.[33−37] Furthermore, the crystal structures of Fe(TPP)Cl,[38] $[Fe(TPP)]_2O$,[33,39] Fe(OEP)Cl,[40] and $[Fe(OEP)]_2O$[41] have been analyzed for supramolecular interactions. The structure of the dimers $[Fe(TPP)]_2O$, $[Fe(OEP)]_2O$, and $[Fe(PPIX)]_2$ (β-hematin) are similar, each consisting of a five-coordinate high-spin iron(III) displaced above the mean plane of the porphyrin toward the axially coordinated O atom. Consequently, these structures serve as excellent model complexes to study the structure of hemozoin and provide excellent models to investigate the Raman enhancement mechanism

previously reported for malaria pigment and its synthetic analogue β-hematin at near-IR excitation wavelengths. In this study, we compare excitation profiles for Raman bands of crystalline monomeric Fe(TPP)Cl and Fe(OEP)Cl and of the corresponding dimeric $[Fe(TPP)]_2O$ and $[Fe(OEP)]_2O$ and compare them with β-hematin.

Experimental Section

Compounds. Fe(TPP)Cl and Fe(OEP)Cl were purchased from Sigma Aldrich. $[Fe(TPP)]_2O$ and $[Fe(OEP)]_2O$ were prepared based on the method of Cheng et al.[41] The commercial Fe(TTP)Cl was further purified by careful chromatography (dichloromethane/hexane, 2:1) on silica (R_f 0.7) following the method of Fleischer et al.[42] After evaporation of solvent, Fe(TPP)Cl was isolated as a purple solid (60% yield). β-hematin was prepared as previously described.[10]

Electronic Absorbance Spectra. Electronic absorption spectra of solid-phase samples were recorded using a J&M MSP800 UV−visible spectrometer equipped with a Leica DM4000 M microscope and a ×40 quartz UV−visible objective with a 7 × 7 μm aperture size in the spectral range of 940−500 nm as 20 accumulations using a 1.2 s integration time per accumulation. Solution-phase spectra were recorded using a Carey 100 Bio UV−visible spectrometer and prepared by dissolving the compounds in dichloromethane (Sigma-Aldrich).

FTIR Spectroscopy. FTIR spectra were recorded with a Varian 600-UMA FTIR microscope equipped with a HgCdTe detector and coupled to a Varian 7000 FTIR spectrometer. Spectra were recorded in reflection mode on Kevley "low e" IR-reflective slide substrates (6 cm^{-1} resolution, 128 coadded scans, apodized using a Blackman Harris four-term function and zero filled by a factor of 2).

Resonance Raman Spectroscopy. The samples were milled with K_2SO_4 (analytical grade from UNIVAR) in a quartz mortar in a 1:1 ratio by weight. The mixed solids were smeared onto a silicon wafer, and RR spectra were recorded on a Renishaw system 2000 spectrometer using 413 and 514 nm excitation lines generated by a Spectra Physics Kr^+-Ar^+ Stabilite 2017 laser system, a 633 nm excitation line generated by a Coherent helium−neon laser, and 782 and 830 nm excitation lines generated by diode lasers (Renishaw RM2000) in a backscattering geometry. The laser power on the sample was approximately 39, 130, 160, 500, and 600 μW for the excitation wavelengths 413, 514, 633, 782, and 830 nm, respectively. The system was equipped with an Olympus optical microscope and a Zeiss ×20 objective. Raman spectra were normalized to the ~982 cm^{-1} band from K_2SO_4. All spectra presented have been smoothed before interactive baseline correction using the concave rubber band algorithm in the OPUS software. The 1064 nm spectra were collected using a Nicolet Nexus near-infrared FT-Raman spectrometer. Spectra were recorded with 5 accumulations and 10 s per acquisition.

Crystallographic Calculations. Supramolecular interaction contact distances and angles were calculated with ORTEP-III[43] and are reported with the conventional D−H···A notation or with D−H···(A−A′) notation, where the acceptor position is the midpoint of the A−A′ bond of the relevant aromatic system. Coordinates for Fe(TPP)Cl,[38] $[Fe(TPP)]_2O$,[39] Fe(OEP)Cl,[40] triclinic $[Fe(OEP)]_2O$,[41] and monoclinic $[Fe(OEP)]_2O$[41] were obtained from the Cambridge Structural Database.[44] Refcodes: KANYUT, PPORFE01, TOYRUU, YIKJOR, and YIKJOR01, respectively.

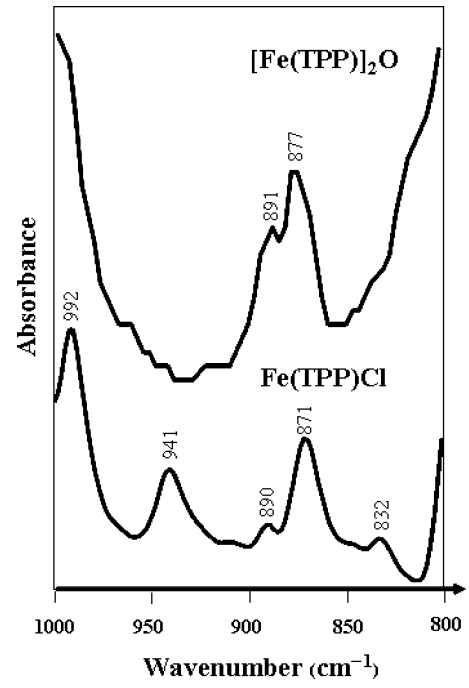

Figure 1. FTIR spectra of Fe(TPP)Cl and $[Fe(TPP)]_2O$.

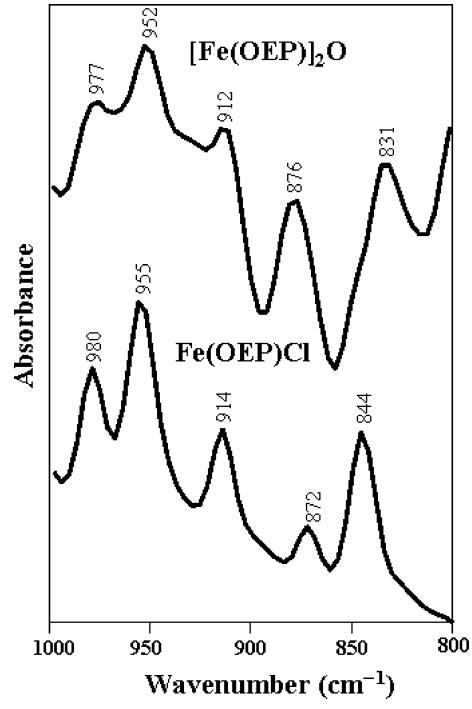

Figure 2. FTIR spectra of Fe(OEP)Cl and $[Fe(OEP)]_2O$.

Results

FTIR Spectroscopy. Oxo-bridged dimers of transition metals including Fe(III) porphyrins were initially characterized with FTIR spectroscopy. The IR absorption region (900−800 cm^{-1}) has been used as evidence for the formation of μ-oxo-bridged dimers for several transition-metal complexes. Figure 1 shows the FTIR spectra of Fe(TPP)Cl and $[Fe(TPP)]_2O$, which are similar to those reported in previous studies.[37,45] Fe(TPP)Cl also has two bands at 890 and 871 cm^{-1}, which have previously been assigned.[37] The peak at 877 cm^{-1} in $[Fe(TPP)]_2O$[42] and the peak at 876 cm^{-1} in $[Fe(OEP)]_2O$[33] (Figure 2) are assigned to the Fe−O−Fe asymmetric stretching mode.

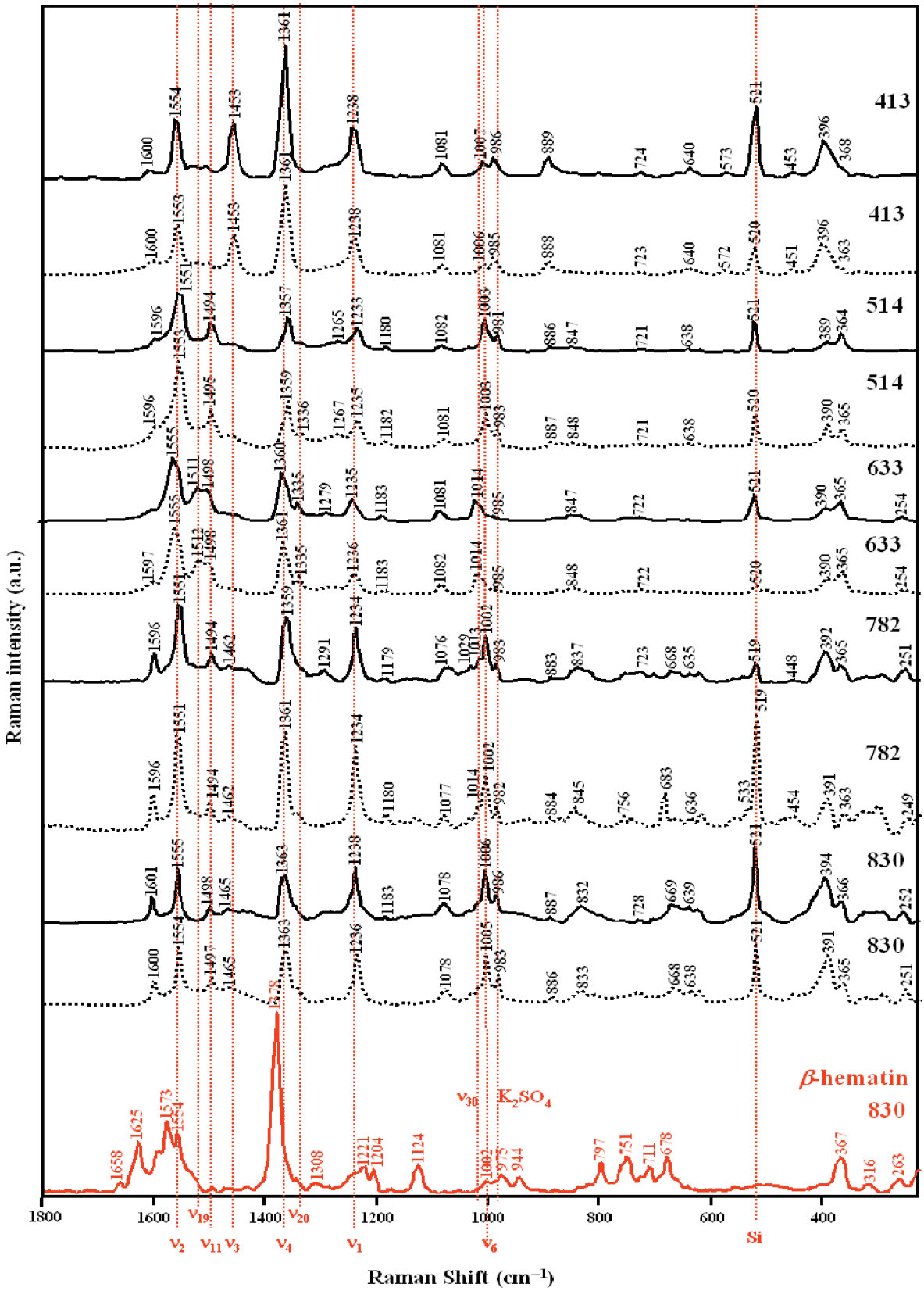

Figure 3. RR spectra of Fe(TPP)Cl, $[Fe(TPP)]_2O$, and β-hematin. The solid lines correspond to the μ-oxo dimer array, and the dashed lines correspond to the chloro monomer.

Solid-State Resonance Raman Spectroscopy. Figures 3 and 4 compare the solid-state RR spectra of monomers and dimers of Fe(TPP) and Fe(OEP) along with β-hematin at different excitation wavelengths, while Tables S1 and S2 (Supporting Information) give a listing of the observed bands along with relative enhancement at each excitation wavelength. It should be noted that all spectra were normalized to the band at ~982 cm^{-1} from the K_2SO_4 standard. Another consideration when

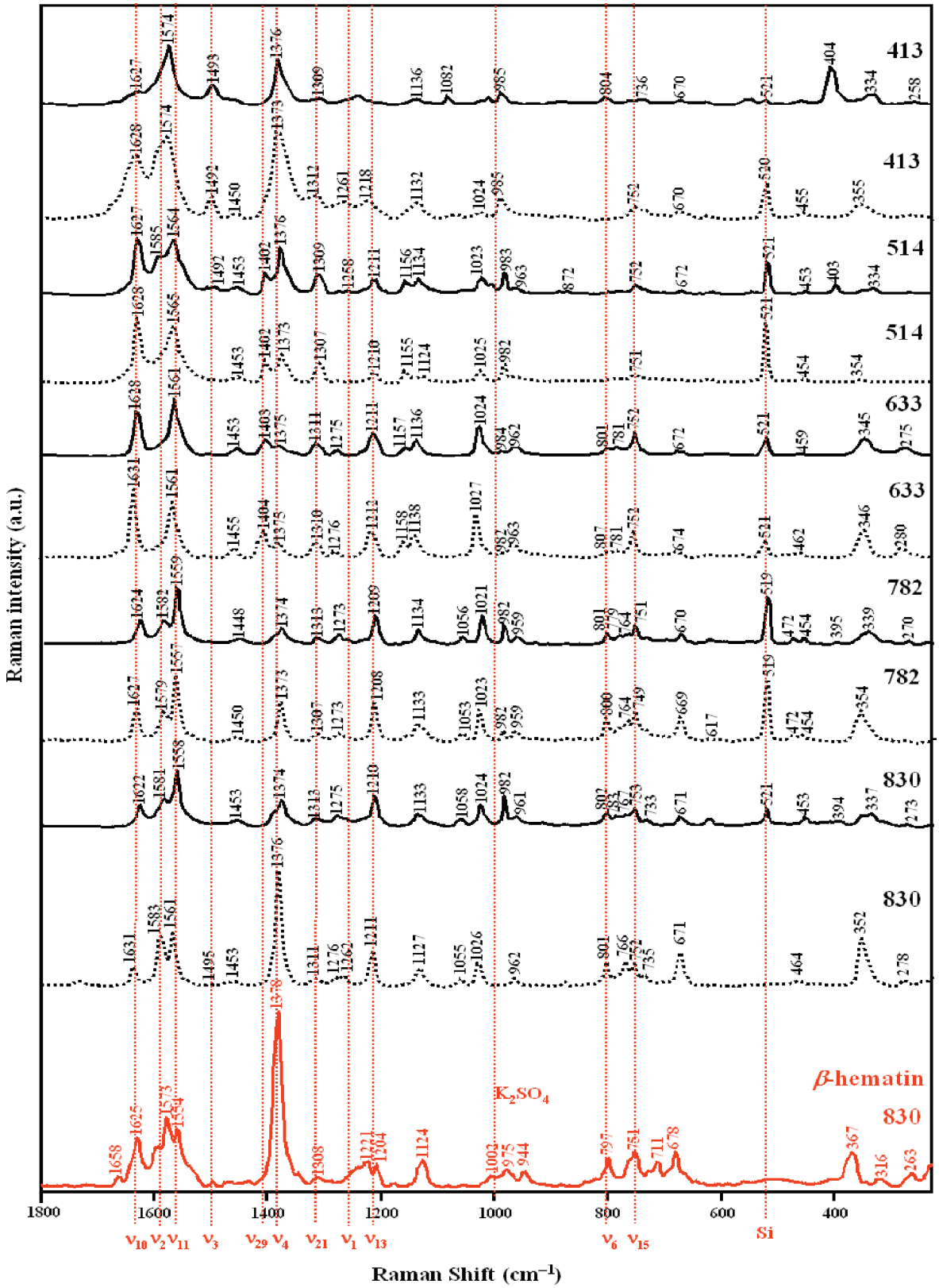

Figure 4. RR spectra of Fe(OEP)Cl, $[Fe(OEP)]_2O$, and β-hematin. The solid lines correspond to the μ-oxo dimer array, and the dashed lines correspond to the chloro monomer.

normalizing spectra is the diminishing quantum efficiency of the detector at the longer excitation wavelengths (830 nm in particular), which can result in wavenumber-dependent intensity changes. To compensate for this, we applied a white light correction to obtain a correction factor to process the spectra. This was performed as an autoroutine using the Renishaw software. We performed all measurements on a silicon wafer and frequency calibrated the spectra to the 520.5 cm^{-1} band.

The vibrational mode notation is based on that proposed by Abe et al.[13] for Ni(OEP) with some amendments to the assignments made by Rush et al.[46] from their studies on Ni(TPP) and a study by Paulet et al.[37] on Fe(TPP)Cl. Although the axial

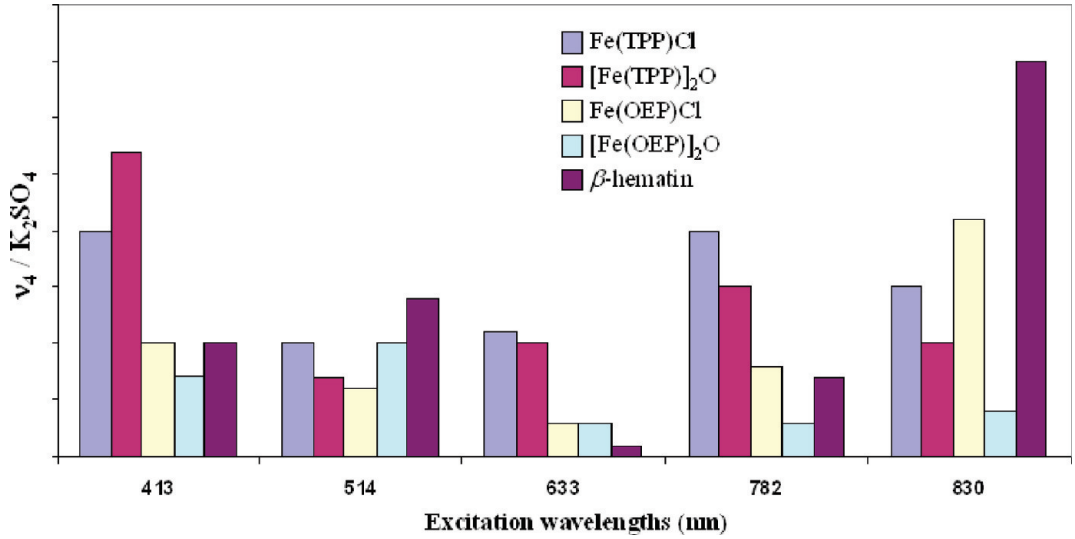

Figure 5. Raman excitation profile showing the ratio of the intensity of ν_4/982 cm^{-1} (K_2SO_4) as a function of excitation wavelength for all compounds investigated.

ligands lower the actual symmetry, the idealized D_{4h} symmetry selection rules are followed closely enough to maintain the assignment scheme.

When exciting into the Soret band using a 413 nm laser, all heme derivatives investigated exhibit dramatic enhancement of the totally symmetric modes including ν_2, ν_3, and ν_4, as expected when the *A* term RR scattering mechanism is the dominant term. Relative enhancement of other A_{1g} modes including ν_1 (in TPPs) and ν_6 (in $[Fe(OEP)]_2O$) are also observed.

When exciting TPPs with 514 nm excitation, the totally symmetric modes ν_2, ν_4, and ν_6 (in the dimer) and the B_{1g} mode ν_{11} in the monomer is also enhanced. However, in OEPs, the nontotally symmetric modes ν_{10}, ν_{11}, ν_{19}, ν_{21}, and ν_{29} dominate the spectra, and the A_{1g} mode ν_4 is also enhanced.

Excitation of TPPs using the 633 nm laser line resulted in the enhancement of many vibrational modes of all different symmetries including polarized (ν_2, ν_4, ν_1), depolarized (ν_{11}, ν_{30}), and inverse polarized modes (ν_{19}, ν_{20}). OEPs, on the other hand, were dominated by B_{1g} (ν_{10}, ν_{11}, ν_{13}, ν_{15}) and A_{2g} (ν_{19}, ν_{21}) modes.

Finally, when using near-IR excitation wavelengths (782 and 830 nm), the spectra of TPPs are still dominated by totally symmetric modes ν_2, ν_4, ν_1, and ν_6. In the spectra of Fe(OEP)Cl, the B_{1g} (ν_{11}, ν_{13}) and A_{1g} (ν_2,) modes are enhanced; however, the A_{1g} ν_4 mode is dramatically enhanced. The spectra of $[Fe(OEP)]_2O$ are dominated by B_{1g} modes ν_{10}, ν_{11}, and ν_{13}, while the ν_4 is relatively weak. Notably, the pattern of the bands in the spectrum at 830 nm of $[Fe(OEP)]_2O$ resembles the FT-Raman spectrum at 1064 nm excitation (Figure S1 in Supporting Information), indicating a lack of type A RR enhancement in this compound relative to the others.

Figure 5 depicts a graph of relative intensity of ν_4/982 cm^{-1} (K_2SO_4) versus excitation wavelength for all compounds investigated including β-hematin. The graph clearly shows the relative intensity of ν_4 for β-hematin, and Fe(OEP)Cl is the greatest when exciting with 830 nm compared to all other excitation wavelengths. Fe(TPP)Cl and $[Fe(TPP)]_2O$ also have high ν_4/982 cm^{-1} (K_2SO_4) ratios at 830 nm, but the intensities are less than the values obtained for 413 nm and 782 excitation. It is clear that the odd compound out is the $[Fe(OEP)]_2O$ dimer, which has a significant ν_4/982 cm^{-1} (K_2SO_4) ratio at 413 nm, but unlike the other compounds, it decreases substantially when exciting with 782 and 830 nm excitation wavelengths.

It is important to note that we were unable to obtain solution-phase RR spectra of Fe(OEP)Cl and Fe(TPP)Cl along with their related μ-oxo dimers when using near-IR excitation wavelengths even at high concentrations (>10 mM) and relatively high laser power. The solution-phase spectra at these excitation wavelengths are swamped by fluorescence and show a broad featureless baseline with no evidence of any bands.

Solid-State and Solution-Phase UV−Visible Spectroscopy. The UV−visible absorption spectra of TPP and OEP derivatives in the solid state are depicted in Figure 6A, while the solution-phase spectra are depicted in Figure 6B. The spectra of the solution- and solid-phase compounds are similar in terms of the position of the Q_v and CT bands; however, the relative intensities are different. The high-spin five-coordinate ferric porphyrins generally display several overlapping bands in the visible region. Assignment of these complex spectra has been controversial.[17,35,47] The optical absorption spectrum of Fe(TPP)Cl in both the solid and solution phases has bands at approximately 513, 577, 651, and 687 nm assigned to the Q_v band and CT bands, respectively.[37] The $[Fe(TPP)]_2O$, on the other hand, has nearly an identical spectrum to that of the monomer in solution but loses intensity of the 651 and 687 nm bands in the solid phase. There is only very weak absorption in the near-IR region for all compounds investigated, with possibly slightly more absorbance in the solid phase compared to that in the solution phase. The solid-phase $[Fe(OEP)]_2O$ dimer has the weakest absorbance in the near-IR region.

X-ray Crystallography. ***(a) General Comments.*** ORTEP-III[43] illustrations of monomeric and dimeric [Fe(TPP)] and [Fe(OEP)] molecules, as they exist in crystal structures, are shown in Figures S2−S6 (Supporting Information). In the previous studies, the structural parameters of interest were primarily the conformational characteristics of the iron atom and porphyrin core, including the bond lengths of Fe−N and Fe axial ligand as well as the displacement of the iron atom out of the porphyrin plane. From the X-ray crystallographic results, these features are similar, all showing five-coordinate square-pyramidal geometry in the high-spin ferric state. Table 1 summarizes the average Fe−N bond distances, Fe(III) displacements from the porphyrin plane, the shortest porphyrin−porphyrin contact distances, and the interplanar angles between the mean 24-atom planes of the molecule.

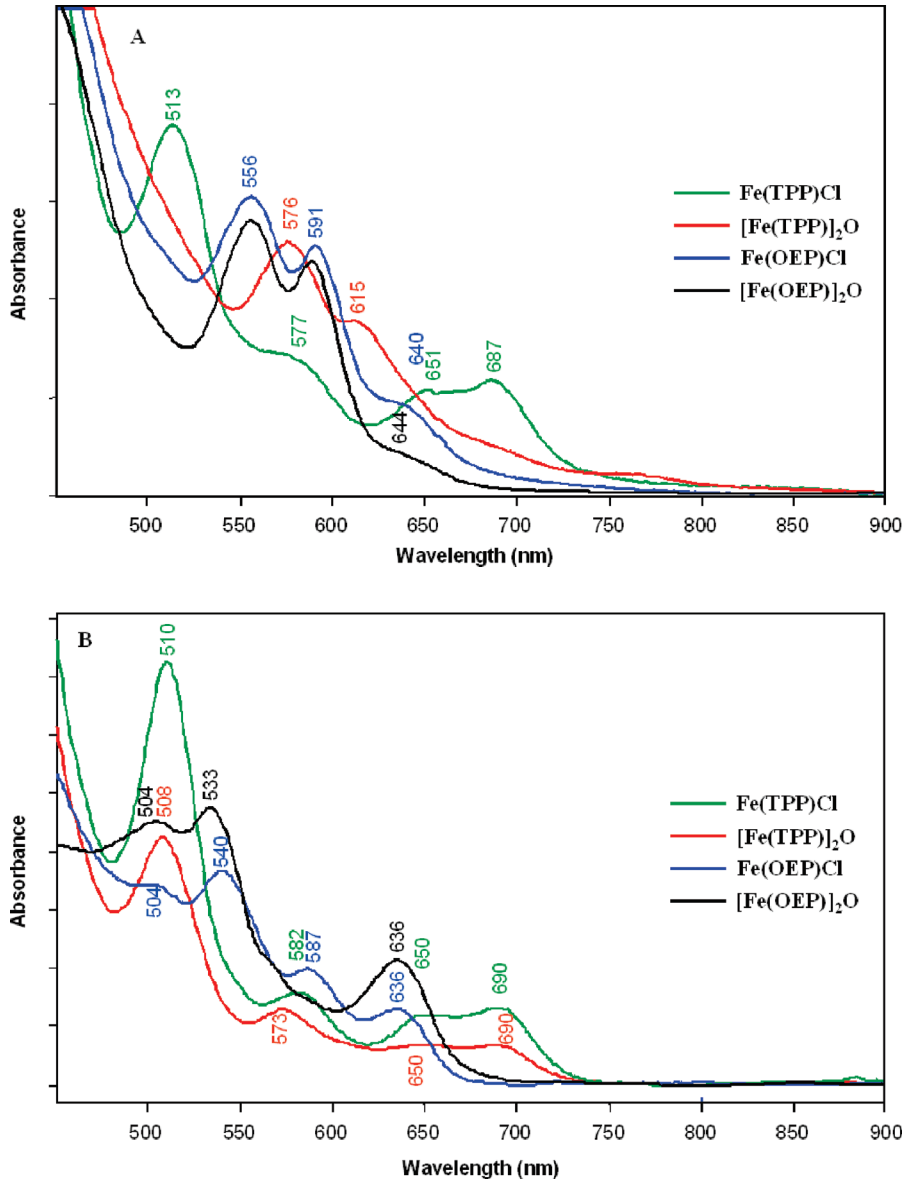

Figure 6. (A) UV−visible absorbance spectra of heme derivatives in the solid phase. (B) UV−visible absorbance spectra of heme derivatives in solution.

The fact that $[Fe(OEP)]_2O$ does not exhibit the enhancement of the electron density marker band ν_4 at near-IR excitation wavelengths reveals that there should be an additional parameter(s) contributing to the RR enhancement mechanisms. To further investigate the mechanism of enhancement of totally symmetric modes, a detailed analysis of the crystal structures is required. We have considered the supramolecular chemistry of TPP and OEP derivatives as a possible factor to explain the enhancement of totally symmetric modes (particularly at near-IR excitation wavelengths). Since the axial ligands and the peripheral substituent groups are different in monomers and dimers of Fe(TPP) and Fe(OEP), their intermolecular interactions may also be different, which in turn could affect the excitonic interactions throughout the arrays. In the following, the various intra- and intermolecular interactions are considered and support the hypothesis that supramolecular interactions are one factor in explaining the enhancement of A_{1g} modes in TPPs and the OEP monomer and the dramatic reduction of the same modes in the OEP dimer. The number of noncovalent intermolecular interactions for the heme compounds in this study are also included in Table 1.

(b) Distance between Porphyrin Planes. In the case of dimeric β-hematin, the closest intermolecular distance between porphyrin planes is 3.4 Å (Diamond[48] calculation; Figure S7, Supporting Information). The average mean plane separations between two porphyrin rings for the Fe(TPP) and Fe(OEP) monomers and dimers are all greater than 4 Å (Table 1), indicating minimal $\pi-\pi$ interactions between the two chromophores in these compounds. However, in the case of the triclinic Fe(OEP) dimer, the geometric constraints of the nearly eclipsed porphyrin cores along with an Fe−O−Fe angle of 172° leads to porphyrin−porphyrin contact distances between the nonparallel cores as short as 3.8 Å.

(c) Delocalized π System and Steric Interaction. The appearance of enhancement of Raman bands assignable to internal modes of the phenyl rings, in resonance with the porphyrin $\pi-\pi^*$ transition, demonstrates an interaction between the phenyl and porphyrin π systems previously attributed to intramolecular delocalization between the porphyrin and phenyl π systems.[49,50] However, since the phenyl rings are tilted with respect to the porphyrin ring (by angles from 53 to 83°) and there is a substantial barrier to rotation, reflecting the steric hindrance

TABLE 1: Molecular Parameters Including Intermolecular Distance and Interactions for Heme Compounds in This Study

heme derivatives	d[Fe−N] (Å)	displacement of Fe (Å)	intermolecular distance between nearest porphyrin rings	interplanar angles between the mean 24-atom planes of a molecule (deg)	type of interaction[a]	enhancement of the ν_4 band (C_α−N, ~1375 cm^{-1}) at near-IR excitation laser
Fe(TPP)Cl monomer[38] $P2_1/n$, $Z = 4$	2.070(9)	0.57	4.5 (by Diamond[48])	0 (by Diamond[48])	C−H···Cl (3), C−H···$\pi_{pyrrole}$ (10), C−H···π_{phenyl} (1)	yes
[Fe(TPP)]$_2$O dimer[33] $C2ca$, $Z = 4$	2.087(3)	0.54	~5.20		C−H···$\pi_{pyrrole}$ (18), C−H···π_{phenyl} (6)	yes
Fe(OEP)Cl monomer[40] $P2_1/c$, $Z = 4$	2.071(2)	0.49	4.02		C−H···Cl (4), C−H···$\pi_{pyrrole}$ (11)	yes
[Fe(OEP)]$_2$O dimer[41] $P-1$, $Z = 4$ $P2_1/c$, $Z = 4$	2.077(3) for triclinic, 2.080(5) for monoclinic	0.50 for triclinic, 0.54 for monoclinic	4.5 for triclinic, 4.6 for monoclinic	7.3 for triclinic, 2.7 for monoclinic	C−H···$\pi_{pyrrole}$ (6) for triclinic and monoclinic	no
β-hematin dimer[4] $P-1$, $Z = 2$	2.061	0.47	3.4 (by Diamond[48])	0 (by Diamond[48])	C−H···O (17)[b], O−H···O (2), C−H···$\pi_{pyrrole}$ (24)	yes

[a] The numbers in parentheses refer to the number of calculated interactions based on d[H···A] ≤ 3.0 Å and d[D···A] ≤ 4.0 Å (except for A = N; d[H···A] ≤ 3.2 Å). [b] The calculated interactions of β-hematin are only calculated at d[D···A] ≤ 4.0 Å since hydrogen atoms were not included in the original paper. See Tables S4−S9 (Supporting Information) for full listings of the calculated H-bond parameters.

between the *ortho*-hydrogen atoms of the phenyl groups and the adjacent pyrrole rings, overlap between the phenyl and porphyrin π systems in the ground state has been questioned.[49,51] It is also significant that the enhancement observed here is a solid-state effect. NMR evidence for phenyl ring rotation in solution from five-coordinate para-substituted phenyl analogues finds an activation barrier of about 16 kcal mol^{-1} for chloro iron(III) analogues and also facilitation of the averaging of nonequivalent phenyl ring ortho protons by addition of chloride ion to the solution,[49] suggesting that a dissociation mechanism is also operating to average the nonequivalent *ortho*-hydrogen atoms. Furthermore, rotation of the phenyl rings in the solid state would be expected to destroy the crystal lattice, as occurs with as little as 35° rotation of axial pyridines in the perchlorate salt of [Fe(OEP)(3-Clpy)$_2$]$^+$ to achieve an $S = 3/2$ (quantum-admixed intermediate spin state)[52] to $S = 1/2$ (low spin state)[53] transition, where the transition is accompanied by fragmentation of the crystal.

In any case, the fact that the aliphatic substituents on Fe(OEP)Cl do not allow the possibility of extended delocalization and yet Fe(OEP)Cl exhibits enhancement of A_{1g} modes at near-IR excitation indicates that there should be other factors that account for the RR enhancement of the ν_4 band. Further, the lack of enhancement in the solution-phase RR spectra even at high concentrations for all heme derivatives investigated to date when using near-IR excitation wavelengths suggests that the enhancement is not due to an intramolecular mechanism. This provides supporting evidence that the band enhancement observed when applying near-IR excitation is a solid-state phenomenon involving intermolecular interactions.

(d) Hydrogen Bonding. β-hematin shows the enhancement of A_{1g} modes at near-IR excitation wavelengths.[10] The interpretation of the high-resolution powder diffraction data indicates that β-hematin contains centrosymmetric dimers with reciprocal propionate linkages and that the dimers are linked together by strong hydrogen bonds.[4] TPPs exhibit hydrogen bond interactions including C−H···π (π system of phenyl and/or porphyrin rings) and C−H···Cl (in the monomer), as shown in Figures 7 and 8. Both OEP derivatives also show hydrogen bond interactions between the porphyrin π systems and C−H of the methylene and methyl groups (Figure 9) and numerous C−H···Cl bonding interactions in the monomer (Figure 10). The total number of C−H···X intermolecular interactions (included in Table 1) for the Fe(OEP) monomer and both the Fe(TPP) monomer and dimer is much larger than that for the Fe(OEP) dimer.

Discussion

The critical finding in this study is that of the five-coordinate high-spin heme compounds investigated, only [Fe(OEP)]$_2$O does not show the enhancement of ν_4 when exciting with near-IR excitation wavelengths. The enhancement of ν_4 when applying near-IR excitation is a solid-state effect that is not observed in the solution phase even at high concentrations (10 mM) for any of the heme derivatives investigated. By analyzing the X-ray crystal structures, using ORTEP-III[43] calculations, the main difference between the compounds that did show the enhancement of ν_4 and those that did not is the number of intermolecular noncovalent bonds. [Fe(OEP)]$_2$O has a total of 6 noncovalent bonds compared to Fe(TPP)Cl (14), [Fe(TPP)]$_2$O (22), Fe(OEP)Cl (15), and β-hematin (43). We hypothesize that the number of noncovalent bonds is an important factor in enabling through-space energy interactions to occur in the solid state of some heme complexes. The Raman intensities, to an extent, reflect

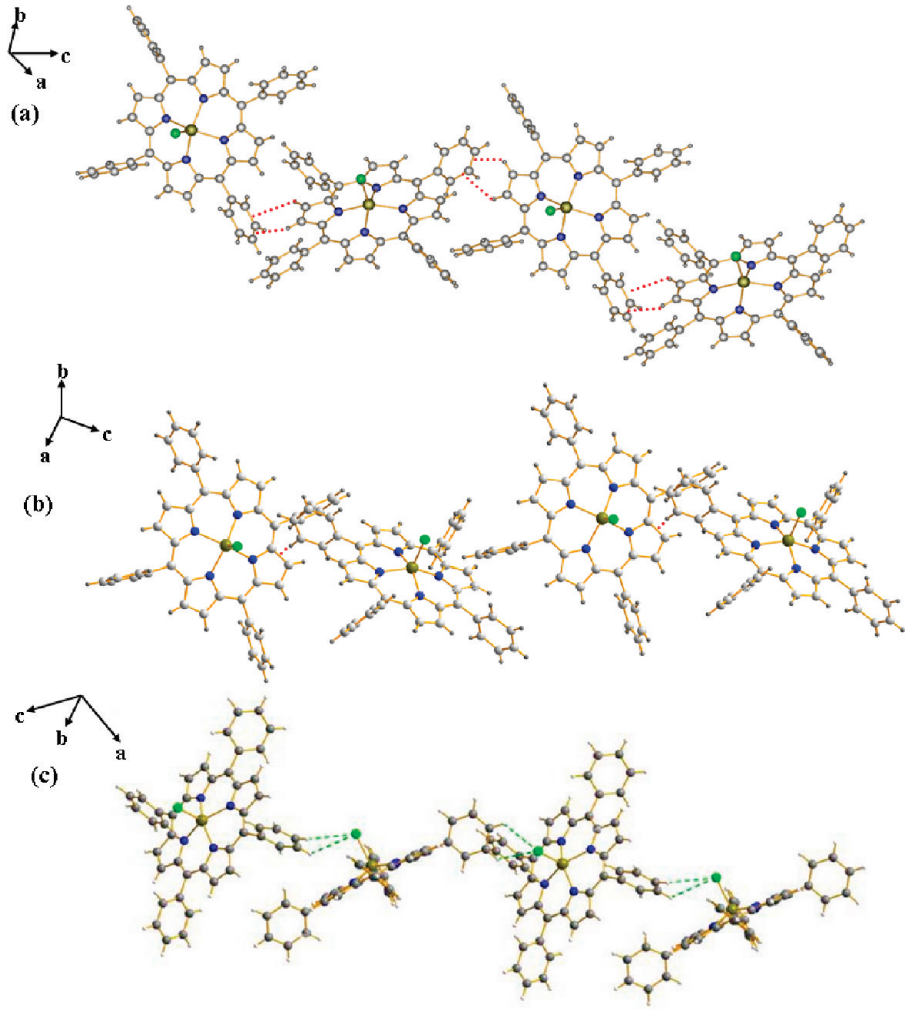

Figure 7. Diamond diagram of Fe(TPP)Cl showing (a) the C−H···π_{phenyl}, (b) C−H···$\pi_{pyrrole}$, and (c) C−H···Cl hydrogen bond interactions.

these interactions, and thus, β-hematin, which has the most noncovalent interactions (43) compared to the other compounds investigated, therefore, also shows the strongest enhancement of ν_4. This is in direct contrast to $[Fe(OEP)]_2O$, which has only six noncovalent bonds, and thus, ν_4 is barely discernible when exciting with near-IR excitation wavelengths. There is not a direct correlation between the intensity of ν_4 and the number of noncovalent interactions because $[Fe(TPP)]_2O$ has the second most interactions (22) but the fourth highest ν_4/982 cm^{-1} (K_2SO_4) when exciting with 830 nm excitation. We argue that a general relationship exists such that when there are significant numbers of noncovalent interactions, there is an increase in the intensity of ν_4. Of course, the real situation is somewhat more complicated than only the number of interactions, and a better measure may be the overall sum of the strengths of the interactions. The current level of available calculations has difficulty in accurately evaluating strengths of the individual weak supramolecular interactions, and such a measure is beyond the scope of this analysis.

In an earlier study,[10] we suggested that the large relative intensity of ν_4 compared to all other bands observed in the spectrum of β-hematin when exciting with near-IR laser lines is the result of excitonic interactions in the heme array. The excitonic hypothesis was supported by the observation of a small electronic transition centered at 867 nm that exhibited a small red shift upon the formation of β-hematin from hematin. Similar enhancement of these modes was also observed for the monomeric precursors, hemin and Fe(PPIX)OH (hematin), but not as much as that observed in the dimer complex, indicating less interaction between porphyrins in monomeric forms.[10] On the basis of symmetry arguments and UV−visible spectroscopic monitoring of the acidification of hemin to β-hematin, which shows a red shifting of the Soret, Q, and a band at ~867 nm, it was hypothesized that an excitonic mechanism is contributing to the observed enhancement.[10] In this study, the compounds investigated showed no definitive evidence of optical transitions in this region for both the solid and solution phases. However, close inspection of the near-IR region indicated some very broad features that may be attributable to electronic transitions in both the solid- and solution-phase spectra. We also performed calculations using TD-DFT on Fe(TPP)Cl and assigned two transitions in the near-IR at 890 and 928 nm (Table S3 and Figure S8 Supporting Information). There appeared slightly more absorption in the near-IR region for the solid-phase compounds compared to that of the solution-phase compounds, but no definitive molecular exciton band was observed in the solid phase. Interestingly, $[Fe(OEP)]_2O$ showed the weakest absorption in this region, which correlates with the compound having the weakest ν_4 band. The lack of any definitive observable molecular exciton band in the solid-phase electronic spectra in the near-IR is not surprising if the molecular orbital overlap is weak. Most of the previous studies regarding the effects of aggregation on absorption spectra of porphyrins have focused on Soret and Q band regions. Since the exciton interaction depends on the square of the transition moment, generally the excitonic effects (including splitting of bands) in

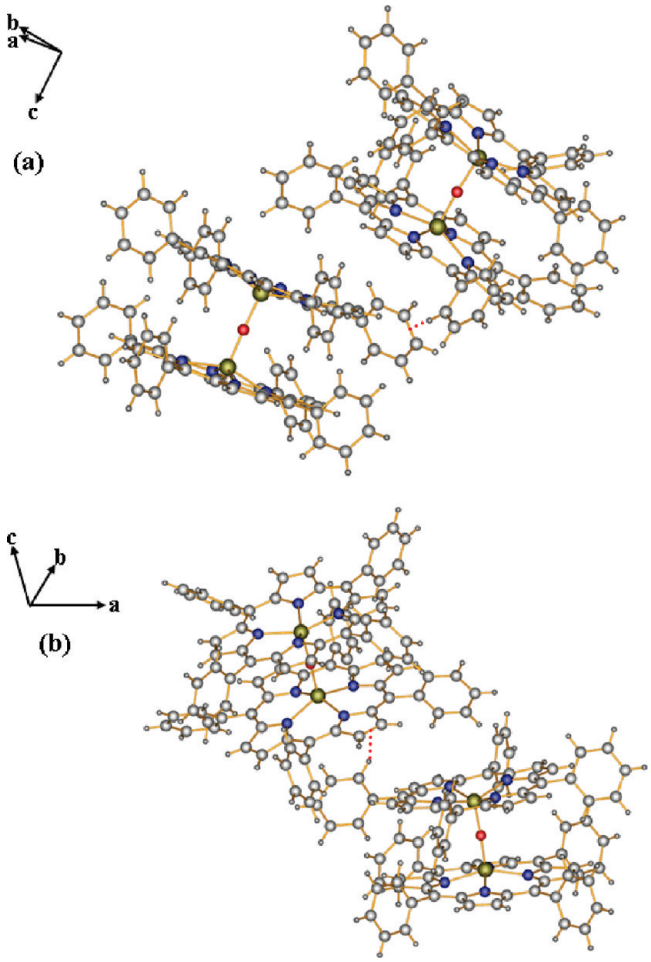

Figure 8. Diamond diagram of $[Fe(TPP)]_2O$ showing (a) the C−H···π_{phenyl} and (b) C−H···$\pi_{pyrrole}$ hydrogen bond interactions.

the visible region are substantially less than those in the near-UV. An early study reported UV−visible spectra of Fe(TPP)Cl recorded under vacuum on a thin-layer optical cell, which clearly showed an unassigned band at 870 nm.[54] Recently, Paulat and Lehnert[55] assigned in detail the magnetic circular dichroism (MCD) and UV−visible bands of Fe(TPP)Cl using TD-DFT. The TD-DFT calculations predict a charge-transfer (CT) transition in high-spin Fe(TPP)Cl at 837 nm, which is an almost pure excited state (82% CT character). The transition at 811 nm corresponds to $A_{1u}\langle 79\rangle \rightarrow d_{xy}$ (90% contribution) with about 10% CT character. Correspondingly, this feature has almost no absorption intensity because of poor orbital overlap of $A_{1u}\langle 79\rangle$ and d_{xy}. The above analysis indicates that CT bands are expected in the near-IR region of high-spin ferric hemes but are too small to observe because of poor orbital overlap.

To the best of our knowledge, there have been no other reports in the literature on the enhancement of A_{1g} modes at near-IR excited RR spectra of Fe(OEP) and Fe(TPP) porphyrins. However, unusual resonance Raman enhancement has been observed for porphyrin-linked arrays when exciting in the visible region. Akins et al.[23,25,29] reported that in highly conjugated systems such as cyanine dyes and porphyrin arrays, other enhancement effects can also be significant. One such important mechanism is AERS, where bands can become enhanced through excitonic interactions between neighboring chromophores.[23,25,29] In this case, energy in the form of an exciton is transferred either via covalent linkages between chromophores or directly though space via overlapping π orbitals, resulting in the enhancement of particular vibrational modes. The fact

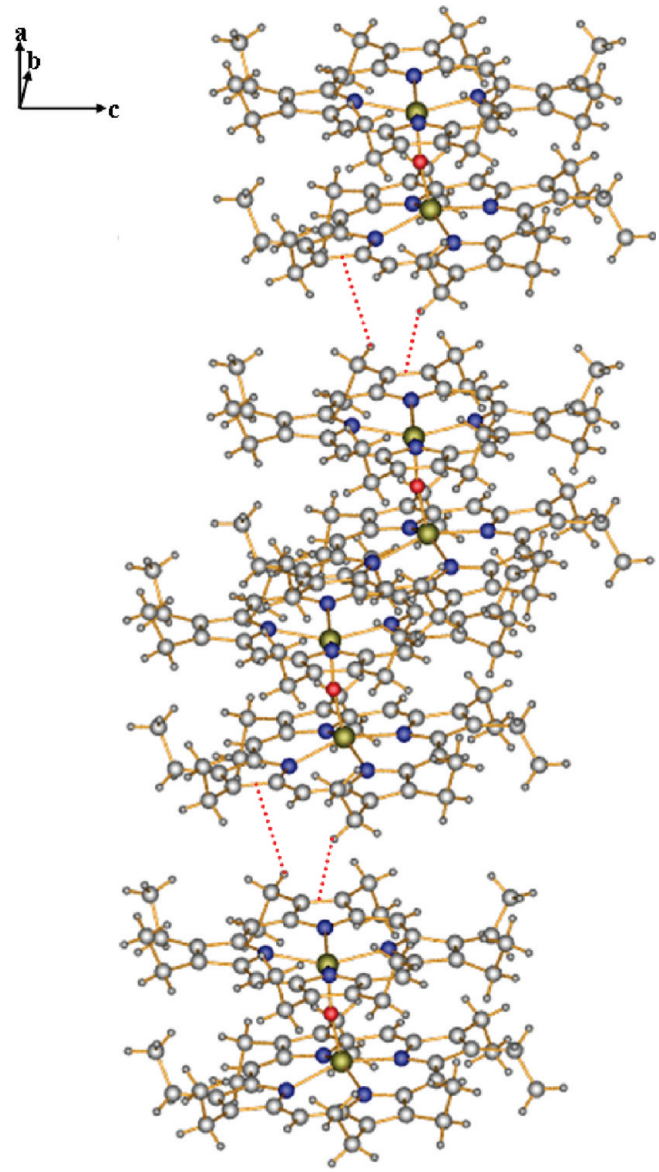

Figure 9. Diamond diagram of $[Fe(OEP)]_2O$ showing C−H···$\pi_{pyrrole}$ hydrogen bond interactions.

that the solution-phase spectra are swamped by fluorescence when using near-IR excitation provides evidence for AERS in the solid state because the net enhancement of Raman vibrational modes in this case may be attributed to an attenuation of fluorescence upon aggregate formation, which is an indicator of AERS.[23] Akins et al.[56] provide an explanation of how bands appearing as a consequence of the *A* term modes can arise from exciton−phonon coupling. They reason that the coupling between lattice vibrations and intramolecular vibrations is the result of electronic charge movement associated with lattice vibrations and charge separation due to vibrations of the individual molecules comprising the aggregate.[56] Exciton−phonon coupling arises from an electron density moment along the direction of aggregation coupling with oscillations of the lattice.[56] They point out that this view is a simplistic representation, and the more correct view is that the allowed lattice oscillations for the electronic distribution are defined by the presence of the exciton.[56] More importantly, they point out that charges interact, which leads to the coupling in the Born−Oppenheimer approximation between electronic and vibrational degrees of freedom.[56] Consequently, the number of

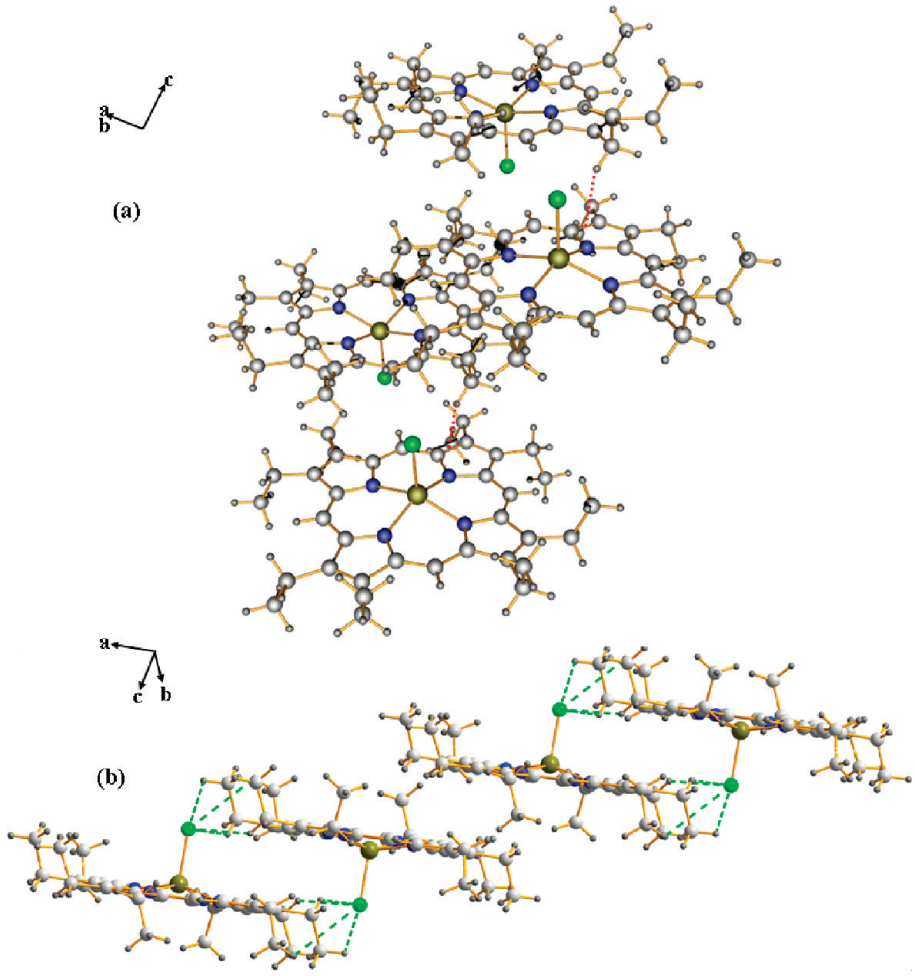

Figure 10. Diamond diagram of Fe(OEP)Cl showing (a) C−H···$\pi_{pyrrole}$ and (b) C−H···Cl hydrogen bond interactions.

charge contacts may be intrinsically important in defining lattice or phonon modes that couple intermolecular and intramolecular vibrations.

To provide more insight into the enhancement mechanism, we utilized additional crystallographic tools to find possible factors involved in the enhancement mechanism. By far, the most compelling difference between the heme compounds that show strong enhancement of A_{1g} modes when irradiating with near-IR excitation wavelengths and the $[Fe(OEP)]_2O$ derivative is the number of intermolecular bonds as deduced by the ORTEP-III[43] calculations. It is hypothesized that the enhancement of some of the A_{1g} modes in β-hematin results from excitonic coupling in the extended heme array through intermolecular interactions. Similarly, the summation of concerted weaker intermolecular interactions between the respective porphyrins appears to be the pivotal factor in explaining the enhancement of totally symmetric A_{1g} modes when exciting with near-IR excitation wavelengths. Fewer noncovalent interactions between porphyrins in the Fe(OEP) dimer may decrease the probability of excitonic interactions in the Fe(OEP) dimer array. Supporting this argument is the indication that simple $\pi-\pi$ intramolecular contact, as between the porphyrin cores of the $[Fe(OEP)]_2O$ dimer, may not be a sufficient condition to enable enhancement. Furthermore, analysis of the angle between heme planes and adjacent porphyrin molecules indicates that the orientation angle is not a critical factor in explaining the enhancement. The interplanar angles between the mean 24-atom planes of a molecule of all heme derivatives except $[Fe(TPP)]_2O$ and Fe(OEP)Cl are shown in Table 1. We can also rule out strong $\pi-\pi$ interactions contributing to the observed enhancement because the $\pi-\pi$ distance is greater than 4 Å.

Conclusions

RR spectra of heme derivatives Fe(TPP)Cl, $[Fe(TPP)]_2O$, and Fe(OEP)Cl reveal a dramatic enhancement of totally symmetric modes (particularly ν_4) at near-IR excitation wavelengths; however, $[Fe(OEP)]_2O$ does not exhibit this feature. The enhancement of the A_{1g} modes in heme porphyrins at near-IR excitation could be interpreted in terms of the presence of intermolecular C−H···X hydrogen bonding, where X is a π system or an electron donor atom. The intermolecular bonding enhances the probability of through-space energy interactions. We can systematically rule out a number of other explanations for the enhancement. (1) The distance between intermolecular porphyrin rings is not a critical factor because both $[Fe(OEP)]_2O$ and Fe(TPP)Cl have the same distance, 4.5 Å, but only Fe(TPP)Cl shows the enhancement. (2) There is no correlation with the translocation distance of the Fe ion from the porphyrin plane and the enhancement (Table 1). (3) There is no correlation with length of the Fe−N bond and the enhancement. (4) There is no correlation between the intermolecular orientation angle and the enhancement.

The relationships that we do see are as follows: (1) The number of noncovalent interactions for either known polymorph of $[Fe(OEP)]_2O$ is relatively few compared to that of the other compounds. Thus, the enhancement of ν_4 may depend on there being a significant number of noncovalent interactions. (2) The

electronic absorption spectra of the solid phase are not conclusive, but there appears to be less absorption in the near-IR region for $[Fe(OEP)]_2O$, which could indicate that the orbital overlap of the molecular exciton band in this compound is particularly weak compared to the other compounds; however, low-temperature magnetic circular dichroism measurements are required to validate these findings.

Our results indicate that the intensity of ν_4 is in part affected by C−H···X hydrogen bonding interactions when X (π, chloro) is an electron-donating entity. This is the first time that hydrogen bonds have been shown to play an important role in RR enhancement. Consequently, the enhancement of ν_4 at near-IR excitation can be used as an indicator of the supramolecular interactions in heme arrays. This study has potential implications in the development of antimalarial drugs that are designed to disrupt hydrogen bond interactions.

Acknowledgment. R.P. acknowledges financial support from the Office of the Commission of Higher Education, Thailand. The authors thank the Monash e-Research Centre and the ITS-Research Support Services for the use of the Monash Sun Grid cluster. We would also like to thank Dr. Evan Robertson (Monash University) for assistance in calculations and Mr. Finlay Shanks for instrument maintenance. This work is supported by an Australian Research Council Discovery Grant.

IUPAC Names

H_2TPP = 5,10,15,20-tetraphenylporphyrin; H_2OEP = 2,3,7,8,-12,13,17,18-octaethylporphyrin; H_2PPIX = 3,8,13,17-tetramethyl-7,12-divinylporphyrin-2,18 dipropionic acid.

Supporting Information Available: Tables S1 and S2: Observed Raman bands (cm^{-1}), assignments, local coordinates, symmetry modes, and relative enhancement factors for -Fe(TPP)Cl, $[Fe(TPP)]_2O$, Fe(OEP)Cl, and $[Fe(OEP)]_2O$ at 413, 514, 633, 782, and 830 nm. Table S3: Assignment of the UV−visible absorption spectra of Fe(TPP)(Cl). Tables S4−S9: The ORTEP-III calculated interactions of Fe(TPP)Cl, $[Fe(TPP)]_2O$, Fe(OEP)Cl, triclinic and monoclinic $[Fe(OEP)]_2O$, and β-hematin. Figure S1: RR spectra of Fe(TPP)Cl, $[Fe(TPP)]_2O$, and $[Fe(OEP)]_2O$ at 1064 nm. Figures S2−S6: ORTEP-III diagrams showing the molecular structure of Fe(TPP)Cl, $[Fe(TPP)]_2O$, Fe(OEP)Cl, and triclinic and monoclinic $[Fe(OEP)]_2O$. Figure S7: β-Hematin molecules in the crystal structure showing the closest porphyrin plane to porphyrin plane contact distance. Figure S8: Contour plots of important molecular orbitals of Fe(TPP)Cl. This material is available free of charge via the Internet at http://pubs.acs.org.

References and Notes

(1) Ridley, R. G. *Nature* **2002**, *415*, 686–693.
(2) Brown, W. H. *J. Exp. Med.* **1911**, *13*, 290–299.
(3) Oliveira, M. F.; Silva, J. R.; Dansa-Petretski, M.; de Souza, W.; Lins, U.; Braga, C. M. S.; Masuda, H.; Oliveira, P. L. *Nature* **1999**, *400*, 517–518.
(4) Pagola, S.; Stephens, P. W.; Bohle, D. S.; Kosar, A. D.; Madsen, S. K. *Nature* **2000**, *404*, 307–310.
(5) Solomonov, I.; Feldman, I.; Baehtz, C.; Kjaer, K.; Robinson, I. K.; Webster, G. T.; McNaughton, D.; Wood, B. R.; Weissbuch, I.; Leiserowitz, L. *J. Am. Chem. Soc.* **2006**, *129*, 2615–2627.
(6) Bohle, D. S.; Conklin, B. J.; Cox, D.; Madsen, S. K.; Paulson, S.; Stephens, P. W.; Yee, G. T. *Am. Chem. Soc. Symp. Ser.* **1994**, *572*, 497–515.
(7) Francis, S.; Sullivan, D. J.; Goldberg, D. *Annu. Rev. Microbiol.* **1997**, *51*, 97–123.
(8) Tilley, L.; Loria, P.; Foley, M.; Ingram, V. M. In *Antimalarial Chemotherapy*; Rosenthal, P. J., Ed.; Humana Press: Totowa, NJ, 2001; pp 87−122.
(9) Webster, G. T.; McNaughton, D.; Wood, B. R. *J. Phys. Chem. B* **2009**, *113*, 6910–6916.
(10) Wood, B. R.; Langford, S.; Cooke, B. M.; Lim, J.; Glenister, F. K.; Duriska, M.; Unthank, J.; McNaughton, D. *J. Am. Chem. Soc.* **2004**, *126*, 9233–9239.
(11) Wood, B. R.; Langford, S. J.; Cooke, B. M.; Lim, J.; Glenister, F. K.; McNaughton, D. *FEBS Lett.* **2003**, *554*, 247–252.
(12) Spiro, T. G.; Li, X.-Y. In *Biological Applications of Raman Spectroscopy*; Spiro, T. G., Ed.; Wiley: New York, 1988, pp. 1−38.
(13) Abe, M.; Kitagawa, T.; Kyogoku, K. *J. Chem. Phys.* **1978**, *69*, 4526–4534.
(14) Hu, S.; Smith, K. M.; Spiro, T. G. *J. Am. Chem. Soc.* **1996**, *118*, 12638–12646.
(15) Spiro, T. G.; Strekas, T. C. *J. Am. Chem. Soc.* **1974**, *96*, 338–345.
(16) Yamamoto, T.; Palmer, G. *J. Biol. Chem.* **1973**, *248*, 5211–5213.
(17) Strekas, T. C.; Packer, A. J.; Spiro, T. G. *J. Raman Spectrosc.* **1973**, *1*, 197–206.
(18) Strekas, T. C.; Spiro, T. G. *J. Raman Spectrosc.* **1973**, *1*, 387–392.
(19) Kramers, H. A.; Heisenberg, W. *Z. Phys.* **1925**, *31*, 681–707.
(20) Dirac, P. A. M. *Proc. R. Soc. London* **1927**, *114*, 710–728.
(21) Albrecht, A. C. *J. Chem. Phys.* **1961**, *34*, 1476–1484.
(22) McHale, J. L. In *Handbook of Vibrational Spectroscopy*; Chalmers, J. M., Griffiths, P. R., Eds.; Wiley: New York, 2002, 534−556.
(23) Akins, D. L. *J. Phys. Chem.* **1986**, *90*, 1530–1534.
(24) Akins, D. L. *J. Colloid Interface Sci.* **1982**, *90*, 373–379.
(25) Akins, D. L.; Özcelik, S.; Zhu, H.-R.; Guo, C. *J. Phys. Chem.* **1996**, *100*, 14390–14396.
(26) Akins, D. L.; Özcelik, S.; Zhu, H.-R.; Guo, C. *J. Phys. Chem.* **1997**, *101*, 3251–3259.
(27) Akins, D. L.; Zhu, H.-R.; Guo, C. *J. Phys. Chem.* **1994**, *98*, 3612–3618.
(28) Akins, D. L.; Akpabli, C. K.; Li, X. *J. Phys. Chem.* **1989**, *93*, 1977–1984.
(29) Akins, D. L.; Lombardi, J. R. *Chem. Phys. Lett.* **1987**, *135*, 495–500.
(30) Akins, D. L.; Macklin, J. W.; Zhu, H.-R. *J. Phys. Chem.* **1992**, *96*, 4515–4521.
(31) Akins, D. L.; Zhu, H.-R. *Langmuir* **1992**, *8*, 546–550.
(32) Akins, D. L.; Zhu, H.-R.; Guo, C. *J. Phys. Chem.* **1996**, *100*, 5420–5425.
(33) Hoffman, A. B.; Collins, D. M.; Day, V. W.; Fleischer, E. B.; Srivastava, T. S.; Hoard, J. L. *J. Am. Chem. Soc.* **1972**, *94*, 3620–3626.
(34) Adar, F.; Srivastava, T. S. *Proc. Natl. Acad. Sci. U.S.A.* **1975**, *72*, 4419–4424.
(35) Burke, J. M.; Kincaid, J. R.; Spiro, T. G. *J. Am. Chem. Soc.* **1978**, *100*, 6077–6083.
(36) Kowalewski, P.; Merlini, J. C.; Bremard, C.; Moreau, S. *J. Mol. Struct.* **1988**, *175*, 55–60.
(37) Paulat, F.; Praneeth, V. K. K.; Nather, C.; Lehnert, N. *Inorg. Chem.* **2006**, *45*, 2835–2856.
(38) Scheidt, W. R.; Finnegan, M. G. *Acta Crystallogr., Sect. C* **1989**, *45*, 1214–1216.
(39) Swepston, P. N.; Ibers, J. A. *Acta Crystallogr., Sect. C* **1985**, *41*, 671–673.
(40) Senge, M. O. *Acta Crystallogr., Sect. E* **2005**, *61*, 399–400.
(41) Cheng, B.; Hobbs, J. D.; Debrunner, P. G.; Erlebacher, J.; Shelnutt, J. A.; Scheidt, W. R. *Inorg. Chem.* **1995**, *34*, 102–110.
(42) Fleischer, E. B.; Srivastava, T. S. *J. Am. Chem. Soc.* **1969**, *91*, 2403–2405.
(43) Burnett, M. N.; Johnson, C. K. *ORTEP-III: Oak Ridge Thermal Ellipsoid Plot Program for Crystal Structure Illustrations*, Report ORNL-6895; Oak Ridge National Laboratory: Oak Ridge TN, 1996.
(44) *Cambridge Structural Database*, version 5.27; Updates August 2006.
(45) Sadasivan, N.; Eberspaecher, H. I.; Fuchsman, W. H.; Caugey, W. S. *Biochemistry* **1969**, *8*, 534–541.
(46) Rush, T. S.; Kozlowski, P. M.; Piffat, C. A.; Kumble, R.; Zgierski, M. Z.; Spiro, T. G. *J. Phys. Chem. B* **2000**, *104*, 5020–5034.
(47) Paulat, F.; Berto, T. C.; George, S. D.; Goodrich, L.; Praneeth, V. K. K.; Sulok, C. D.; Lehnert, N. *Inorg. Chem.* **2008**, *47*, 11449–11451.
(48) *Crystal Impact. DIAMOND*, version 3.1.; Crystal Impact GbR: Bonn, Germany, 2006.
(49) Fuchsman, W. H.; Smith, Q. R.; Stein, M. M. *J. Am. Chem. Soc.* **1977**, *99*, 4190–4192.
(50) Eaton, S. S.; Eaton, G. R. *J. Am. Chem. Soc.* **1975**, *97*, 3660–3666.
(51) Tsubaki, M.; Srivastava, R. B.; Yu, N. T. *Biochemistry* **1982**, *21*, 1132–1140.
(52) Scheidt, W. R.; Geiger, D. K.; Hayes, R. G.; Laing, G. *J. Am. Chem. Soc.* **1983**, *105*, 2625–2632.
(53) Scheidt, W. R.; Geiger, D. K.; Haller, K. J. *J. Am. Chem. Soc.* **1982**, *104*, 495–499.
(54) Felton, R. H.; Owen, G. S.; Dolphin, D. In *The Chemical and Physical Behaviour of Porphyrin Compounds and Related Structures*; Adler, A. D., Ed.; New York, 1973; Vol. 206, pp 504−515.
(55) Paulat, F.; Lehnert, N. *Inorg. Chem.* **2008**, *47*, 4963–4976.
(56) Akins, D. L.; Zhuang, Y. H.; Zhu, H.-R.; Liu, J. Q. *J. Phys. Chem.* **1994**, *98*, 1068–1072.

JP102307S